Mon. Not. R. Astron. Soc. **277**, 458–470 (1995)

Ultra-high-resolution observations of the intrinsic line profiles of interstellar CH, CH^+ and CN

I. A. Crawford

Department of Physics and Astronomy, University College London, Gower Street, London WC1E 6BT

Accepted 1995 June 7. Received 1995 May 2; in original form 1995 March 24

ABSTRACT

Ultra-high-resolution (0.3 km s^{-1} FWHM) observations of interstellar CH and CH^+ are presented for five southern stars (HD 110432, 152234, 152235, 152236 and 152270); CN spectra were also obtained for HD 152236 and 152270, and Ca K and K I spectra for HD 110432. These observations have enabled us to resolve the intrinsic line profiles towards these stars for the first time, and have made possible the accurate measurement of the velocity dispersions (*b*-values) of the various atomic and molecular velocity components. The line profiles are found to be inconsistent with shock theories for the production of CH^+ in diffuse molecular clouds, and favour the view that this molecule is produced in warm ($T \gtrsim 2000$ K) gas at the interfaces between cool dense clouds and the hot interior of the Sco–Cen bubble. In the case of one star (HD 152270) the *b*-value measurements conclusively demonstrate an onion-shell-like structure for the absorbing cloud, with CN occurring in the coolest/least turbulent region (presumably the deep interior), CH in a somewhat hotter/more turbulent region (presumably the outer regions), and CH^+ in the warmest/most turbulent region of all (as expected for an interface with a hot intercloud medium.

Key words: line: profiles – ISM: clouds – ISM: molecules.

1 INTRODUCTION

Almost all existing studies of interstellar molecular absorption lines have been performed using instruments which lack the spectral resolution required to determine the intrinsic line profiles accurately. This is because most existing high-resolution optical spectrographs have resolving powers $R(\equiv \lambda/\Delta\lambda) \lesssim 10^5$, corresponding to instrumental profiles $\gtrsim 3$ km s^{-1} (FWHM). A linewidth of 3 km s^{-1} corresponds to kinetic temperatures of 2550 K for CH/CH^+, and 5100 K for CN, and, as these molecules (with the possible exception of CH^+) are expected to occur in much colder regions, the thermal linewidths are usually much narrower than the instrumental resolution. Moreover, while it is known that internal cloud turbulence broadens interstellar line profiles over the thermal value, this broadening is also generally less than the instrumental resolution of existing spectrographs. The importance of being able to resolve the intrinsic line profiles has been discussed in detail by Black & van Dishoeck (1988).

Work at significantly higher resolution has so far been restricted to the interstellar sightline towards ζ Oph, for which Lambert, Sheffer & Crane (1990) obtained spectra with $R = 6 \times 10^5$ using the coudé echelle spectrograph at the McDonald Observatory, and Crawford et al. (1994) obtained spectra with $R = 9 \times 10^5$ using the new Ultra-High-Resolution Facility (UHRF) at the AAT. These observations have revealed the intrinsic molecular line profiles towards this much-studied star, yielding important information on the physical conditions in the foreground clouds. However, they also revealed the presence of two closely spaced velocity components (separation 1.13 ± 0.10 km s^{-1}), which means that this sightline is not, after all, the best candidate for testing line-profile predictions made by theoretical models of diffuse interstellar clouds. Given the atypical nature of the ζ Oph sightline, in this and other respects, it is clearly of interest to extend very high-resolution studies to other lines of sight.

Here we describe UHRF observations ($R = 9.6 \times 10^5$) of interstellar CH and CH^+ towards five southern stars. Two of these stars have also been observed in CN, and one in the atomic species Ca II and K I. Table 1 lists the lines observed, together with the rest wavelengths and oscillator strengths adopted in the analysis. The principal objective was to measure the intrinsic linewidths, in order to place firm limits on the kinetic temperatures in the absorbing clouds, and to test the various theories advanced for CH^+ production in diffuse clouds.

Table 1. Interstellar lines observed in the present study.

Atom/Mol.	Line	λ (Å) (ref)	f (ref)
CH	$R_2(1)$*	4300.313 (1)	5.06×10^{-3} (1)
CH^+	R(0)	4232.548 (2)	5.50×10^{-3} (2)
CN	R(0)†	3874.607 (1)	3.38×10^{-2} (1)
CN	R(1)‡	3873.999 (1)	2.25×10^{-2} (1)
Ca II	K	3933.663 (3)	6.35×10^{-1} (3)
K I		7698.974 (3)	3.39×10^{-1} (3)

*Split into two Λ-doublet components separated by 20.5 mÅ.
†Actually a blend of the $R_1(0)$ and $^RQ_{21}(0)$ lines.
‡Actually a blend of the $R_1(1)$, $R_2(1)$ and $^RQ_{21}(1)$ lines.
Refs: (1) Black & van Dishoeck (1988); (2) Lambert & Danks (1986); (3) Morton (1991).

1.1 Galactic environment of the observed clouds

The five stars observed here are listed in Table 2. Four of these (HD 152234, 152235, 152236 and 152270) are members of the Sco OB1 association, and their interstellar spectra have been studied previously using the Mt Stromlo coudé echelle spectrograph at a resolving power of $R = 10^5$ (Crawford, Barlow & Blades 1989; Crawford 1989a, 1990). The remaining star, HD 110432, lies in the direction of the Southern Coalsack, and Mt Stromlo coudé spectra have been presented by Crawford (1989b, 1991a).

The Sco OB1 association lies in the Sagittarius spiral arm at a distance of 1900 pc (Humphreys 1978). However, there is considerable evidence (discussed in section 4.7 of Crawford 1992) that the absorbing molecular clouds lie very much closer, probably within a few hundred pc of the Sun. In particular, the low-velocity ($-6 \lesssim v_{\rm helio} \lesssim +6$ km s^{-1}) components most probably arise in outlying gas associated with the Lupus molecular cloud complex at a distance of about 170 pc (Murphy, Cohen & May 1986). This interpretation accounts for the strongest CH and CN (with their associated CH^+) components towards each star. All the Sco OB1 stars except HD 152235 exhibit weaker components at more negative velocities (only detected in CH^+ for HD 152270) and, as discussed by Crawford (1992), these probably lie at greater distances. However, only the most negative-velocity components of all (i.e., the −16 km s^{-1} CH, and associated CH^+, component towards HD 152236, and the −14.8 km s^{-1} CH^+ component towards HD 152270) can be assigned a dynamical distance (≈ 1.3 kpc) as great as the near side Sagittarius arm itself, assuming the Galactic rotation model of Fich, Blitz & Stark (1989).

Although the distance of HD 110432 is rather uncertain (Crawford 1989b), it almost certainly lies well beyond the Coalsack's distance of 170 pc (Rodgers 1960; Franco 1989). There is little doubt, therefore, that the absorption lines observed towards this star arise within molecular gas associated with the Coalsack dust clouds.

It is worth drawing attention to the Galactic environment of these clouds. Both the Lupus complex and the Coalsack form part of a well-defined ridge of molecular clouds identified by Dame et al. (1987; cf. their fig. 7). This feature is over a kiloparsec long, and Dame et al. speculate that it may be associated with the inner edge of the local spiral arm. In the fourth galactic quadrant ($270° < l < 360°$), which includes both the Lupus clouds and the Coalsack, the ridge lies at a distance of about 170 pc, where it forms a backdrop to most of the stars of the Sco–Cen OB association (although some stars, particularly in the upper-Scorpius subgroup, lie beyond it; de Geus, de Zeeuw & Lub 1989). The Sco–Cen association is responsible for the excavation of a large bubble (the Sco–Cen bubble, sometimes also called the Loop I bubble) in the interstellar medium (Cox & Reynolds 1987; de Geus 1992), the interior of which is filled with a very hot ($T \sim 5 \times 10^6$ K), low-density ($n_{\rm H} \sim 2.5 \times 10^{-3}$ cm^{-3}), X-ray-emitting gas (Egger & Aschenbach 1995, and references therein). A map of the fourth quadrant, showing the locations of the molecular clouds, the Sco–Cen association, and the Sco–Cen bubble, is given in fig. 1 of Crawford (1991b). The main point to note is that, given the size and location of the bubble (de Geus 1992), there is little doubt that the hot gas in the interior surrounds, or at least abuts, the cold molecular clouds of the background ridge. As we shall see, this circumstance may be important for an understanding of the origin of the CH^+ associated with these clouds.

1.2 The CH^+ problem

It has long been known that low-temperature equilibrium chemical models are unable to reproduce the CH^+ column densities that are typically observed in diffuse molecular clouds (e.g. Dalgarno 1976; Black 1988). It is known that the reaction

$$C^+ + H_2 \rightarrow CH^+ + H - 0.4\ \text{eV} \qquad (1)$$

is, in principle, able to produce column densities of the observed order of magnitude, but this reaction is endothermic and the 0.4-eV barrier corresponds to a temperature of 4650 K. This is much higher than the temperatures (< 100 K) deduced for diffuse molecular clouds by other methods (see Black & van Dishoek 1991 for a useful summary of diffuse molecular cloud temperatures). One mechanism whereby cloud temperatures can be raised to the values required by reaction (1) is to postulate the propagation of a moderate velocity shock ($v_s \gtrsim 10$ km s^{-1}) through the cloud, in which case the post-shock temperature will be sufficient (several thousand degrees) to overcome the energy barrier (Elitzur & Watson 1978, 1980; Mitchell & Watt 1985; Draine & Katz 1986; Pineau des Forêts et al. 1986). These theories make a number of specific predictions about the line profiles and velocities which may be tested by means of high-resolution spectroscopy, and it is with these that we shall be concerned in the present paper.

The main point is that the shock models predict a significant velocity difference (amounting to several km s^{-1}) between the CH and CH^+. This is because the CH^+ is formed in the hot post-shock gas, where the temperature is sufficient to drive reaction (1) and, in a simple hydrodynamic shock, this material will have been accelerated up to three-quarters of the shock velocity (Elitzur & Watson 1980). On the other hand, most of the other molecules are thought to form in the cold post-shock gas, which will be moving at the shock velocity, but which will have a density several tens of times greater than the hot post-shock gas (e.g. Spitzer 1978; p. 221). Thus, for a line-of-sight perpendicular to the shock

Table 2. List of observations made of interstellar molecular lines using the UHRF. Column 7 gives the total number of continuum electrons above the background for each collapsed 24-μm spectral element. Column 8 gives the measured equivalent widths (errors are 2σ values). For blended velocity components the total equivalent width is given; for HD 152236 two well-resolved CN components are present (cf. Fig. 4), and the equivalent widths of these are listed separately. Column 9 lists the equivalent widths measured from $R = 10^5$ observations obtained at Mt Stromlo (Crawford 1989a, 1990, 1991a), and column 10 gives equivalent widths published by other authors.

Star (HD)	V	$E(B-V)$	Line	U.T. Date	Exposures (n × secs)	Total Counts (e^-)	w_λ (here) (mÅ)	w_λ (Stromlo) (mÅ)	w_λ (other) (ref) (mÅ)
110432	5.4	0.40	CH	22-4-94 27-4-94 29-4-94	3 × 1800 2 × 1800 2 × 1800	2.1×10^4	12 ± 1	13 ± 2	12.7 ± 2.2 (1)
			CH^+	22-4-94 29-4-94	3 × 1800 1 × 1800	8.9×10^3	14 ± 1	14 ± 2	12.4 ± 1.0 (1)
			Ca K	23-4-94	2 × 1800	4.0×10^3	52 ± 1	56 ± 4	...
			K I	24-4-94	2 × 1200	6.0×10^3	77 ± 1	...	...
152234	5.5	0.46	CH	24-4-94	2 × 1800	8.5×10^3	10 ± 1*	5.9 ± 0.9	...
			CH^+	24-4-94	4 × 1800	6.5×10^3	19 ± 1	20 ± 3	...
152235	6.4	0.79	CH	22-4-94	4 × 1800	3.1×10^3	29 ± 1	33 ± 3	...
			CH^+	23-4-94 29-4-94	4 × 1800 2 × 1800	3.6×10^3	42 ± 1	42 ± 5	...
152236	4.8	0.69	CH	11-5-93 22-4-94	2 × 1800 2 × 1800	6.7×10^3	17 ± 1	20 ± 3	19.4 ± 2.8 (1)
			CH^+	23-4-94 28-4-94	4 × 1800 2 × 1800	9.6×10^3	15 ± 1	16 ± 2†	...
			CN R(0)	29-4-94	2 × 1800	6.1×10^3	1.5 ± 0.3 6.0 ± 0.3	1.7 ± 0.9 6.5 ± 0.9	... 6.1 ± 0.6 (2)
			CN R(1)				0.5 ± 0.2 1.9 ± 0.2	... ...	... 2.1 ± 1.2 (2)
152270	6.7	0.48	CH	22-4-94 29-4-94	4 × 1800 2 × 1800	5.0×10^3	9.5 ± 0.5	8.2 ± 1.3	...
			CH^+	23-4-94 29-4-94	5 × 1800 2 × 1800	4.1×10^3	12 ± 1	13 ± 3	...
			CN R(0)	24-4-94 29-4-94	2 × 1800 2 × 1800	2.4×10^3	4.0 ± 0.6	5.8 ± 1.3	...
			CN R(1)				1.4 ± 0.5	...	...

*Includes velocity components not identified by Crawford (1989a).
†Obtained from the spectrum discussed in the 'note added in proof' appended to Crawford (1989a).
Refs: (1) Gredel et al. (1993); (2) Palazzi et al. (1992).

front, we expect a velocity difference of one-quarter of the shock velocity between the CH and CH^+. As the models typically require shock velocities $\gtrsim 12$ km s^{-1}, this velocity shift could be of the order of 3 km s^{-1} or more. If the shock is viewed obliquely, the observed velocity difference will be reduced by a factor cos θ, where θ is the angle between the line of sight and direction of shock propagation. In addition, we might expect some CH to form in the hot gas behind the shock front (i.e., at the same velocity as the CH^+), for which the models of Mitchell & Watt (1985) suggest a column density of $\approx 10^{12}$ cm^{-2}. There is also the possibility that CH may occur in the pre-shock gas if, as argued in Section 1.1 for these stars, this material is largely molecular; such a component would be offset by up to three-quarters of the shock velocity from the CH^+ (again subject to a geometrical projection factor).

In addition to predicting these velocity differences, the shock models also imply that the various components will have different velocity dispersions owing to the different temperatures. For example, a temperature of 4650 K (i.e., that corresponding to the energy barrier of reaction 1) would result in a thermal contribution to the CH^+ *b*-value of 2.4 km s^{-1}. Any CH formed in the shock region would have the same *b*-value. On the other hand, the cold post-shock gas, where most of the other molecules are thought to form, is expected to have a temperature of $\lesssim 100$ K (e.g. Mitchell & Watt 1985), at which temperature the thermal CH *b*-value would be only 0.36 km s^{-1}. Thus, according to these models, not only should the CH and CH^+ lines be displaced from each other by several km s^{-1}, but the CH^+ line profile should be very much broader than the CH (unless the cold post-shock gas is subject to turbulent motions of several km s^{-1}, which would be highly supersonic at 100 K).

It has been recognized for some time that non-magnetic hydrodynamic shocks, as outlined above, are probably unable to produce column densities of CH^+ of the order of 10^{13} cm^{-2} (Mitchell & Watt 1985; Pineau des Forêts et al. 1986). As column densities of this order are commonly observed in interstellar clouds (including those studied here, cf. Table 3), recourse has been had to magnetohydrodynamic (MHD) shocks. These are able to produce CH^+ column densities of the required order of magnitude given interstellar magnetic field strengths of ≈ 5–10 μG and shock velocities of $\gtrsim 10$ km s^{-1} (e.g. Draine & Katz 1986; Pineau des Forêts et al. 1986).

These models make somewhat different predictions for the resulting line profiles, and Draine & Katz (1986, their figs 4 and 5) have performed detailed calculations of these for a range of shock parameters. The main point to note is that, owing to the different response of neutral and ionized species to the presence of a magnetic field, the CH^+ and CH formed in the hot post-shock gas have a significant velocity difference (amounting to 3.5 km s^{-1} for a 10 km s^{-1} shock). On the other hand, these models predict a somewhat smaller velocity difference (about 1.2 km s^{-1}) between the hot CH^+ and any CH which may form in the *cold* post-shock gas (cf. fig. 4 of Draine & Katz 1986). Thus, if the bulk of the CH is formed in the cold post-shock gas, as is generally assumed in the non-MHD case, the MHD models predict a *smaller* velocity difference between the hot CH^+ and the main (cold) CH component than do the non-magnetic shock models, although this velocity difference is still expected to be of the order of 1 km s^{-1}.

In addition to making predictions concerning the line profiles, the shock models make a number of other predictions (for example, concerning the abundance of other molecules, the relationship between CH^+ and optical extinction, and the degree of rotational excitation of H_2). It is now realized that many of these predictions are in conflict with recent observational results (interested readers are referred to the thorough discussion by Gredel, van Dishoeck & Black 1993), and this has led to alternative suggestions for the formation of CH^+. As pointed out by Duley et al. (1992), shocks are not the only means by which the temperature of a molecular gas may be raised to the values needed to drive reaction (1). One of the most promising alternatives, suggested by Duley et al., is the presence of warm boundary layers between cold molecular gas and a hot intercloud medium, while another, advanced by Falgarone & Puget (1995) and Falgarone, Pineau des Forêts & Roueff (1995), involves the dissipation of turbulence in the interiors of diffuse clouds.

2 OBSERVATIONS

A summary of the observations is given in Table 2. All the observations were obtained in 1994 April, apart from a subset of the CH data for HD 152236 obtained in 1993 May. The instrument has been described in detail by Diego et al. (1995). For the 1994 observations, the detector was the AAO Tektronix CCD (1024 × 1024 24-μm pixels), and the spectrograph was operated with a confocal image slicer (Diego 1993). Owing to the very high dispersion of the UHRF (approximately 1 Å cm^{-1}, depending on the wavelength) only a small region (about 2 Å) of the echelle order containing each line was imaged at a time. The CCD output was binned by a factor of 8 perpendicular to the dispersion direction in order to reduce the readout noise associated with extracting the broad spectrum produced by the image slicer (in the configuration adopted here, each order was approximately 10.3 mm wide at the detector, corresponding to 54 binned CCD pixels). The resolution, measured from the observed width of a stabilized He–Ne laser line, was 0.314 ± 0.005 km s^{-1} (FWHM). For the two exposures obtained in 1993 the instrumental set-up was as described by Crawford et al. (1994).

The spectra were extracted from the CCD image using the FIGARO data-reduction package (Shortridge 1988) at the UCL Starlink node. Scattered light was measured from the inter-order region and subtracted. Wavelength calibration was performed using a Th–Ar lamp. Linear fits to the four or five Th–Ar lines identified in the narrow ($\lesssim 2$ Å) spectral coverage of the detector resulted in typical rms residuals of 4×10^{-4} Å (in no case was the rms residual greater than 6×10^{-4} Å). Once wavelength-calibrated, the spectra were converted to the heliocentric velocity frame, and multiple exposures (Table 2) were co-added. The resulting spectra are shown in Figs 1–5.

3 RESULTS

3.1 Equivalent widths

Table 2 lists the equivalent widths of the molecular lines measured here, and compares them with previously published values (total equivalent widths are given, as this quantity is independent of spectral resolution). This comparison is important, given the evidence for uncorrected scattered light found in the very earliest spectra obtained with the UHRF (Crawford et al. 1994; Diego et al. 1995). As described in section 7.3 of Diego et al. (1995), the mode of operation of the instrument has now been modified so as to eliminate this problem. The close agreement between the equivalent widths measured here and those obtained with other instruments shows that this approach has been successful, and that the present spectra are not significantly contaminated by stray light (which would cause the equivalent widths to be underestimated).

Table 3. Line-profile parameters for the lines observed towards the five stars. T_k^{ul} is the upper limit to the kinetic temperature (derived under the assumption that there is no line-of-sight turbulence contributing to the observed linewidths).

Star (HD)	Line	v_{helio} (km s^{-1})	b (km s^{-1})	log N (cm^{-2})	T_k^{ul} (K)
110432	CH	$+2.9 \pm 0.2$	$1.7^{+0.2}_{-0.2}$	$12.70^{+0.05}_{-0.05}$	2270^{+570}_{-500}
		$+6.9 \pm 0.1$	$1.3^{+0.2}_{-0.2}$	$13.02^{+0.05}_{-0.05}$	1330^{+440}_{-380}
	CH^+	$+5.7 \pm 0.1$	$2.3^{+0.2}_{-0.2}$	$13.25^{+0.05}_{-0.05}$	4160^{+760}_{-690}
	Ca K	$+3.5 \pm 0.2$	$1.6^{+0.4}_{-0.3}$	$11.10^{+0.10}_{-0.10}$	6200^{+3500}_{-2100}
		$+5.8 \pm 0.1$	$1.2^{+0.2}_{-0.2}$	$11.78^{+0.07}_{-0.08}$	3500^{+1300}_{-1100}
		$+8.4 \pm 0.1$	$1.1^{+0.3}_{-0.3}$	$11.25^{+0.10}_{-0.15}$	2900^{+1800}_{-1400}
		$+10.4 \pm 0.2$	$0.6^{+0.2}_{-0.2}$	$10.20^{+0.20}_{-0.20}$	870^{+680}_{-480}
	K I	$+1.7 \pm 0.2$	$1.0^{+0.1}_{-0.1}$	$10.60^{+0.05}_{-0.05}$	2360^{+500}_{-450}
		$+3.3 \pm 0.1$	$0.6^{+0.1}_{-0.2}$	$10.55^{+0.10}_{-0.15}$	850^{+510}_{-470}
		$+5.6 \pm 0.2$	$0.9^{+0.2}_{-0.1}$	$11.37^{+0.13}_{-0.12}$	1910^{+940}_{-400}
		$+6.9 \pm 0.1$	$0.7^{+0.1}_{-0.1}$	$11.60^{+0.05}_{-0.10}$	1160^{+350}_{-310}
		$+8.4 \pm 0.3$	$0.8^{+0.7}_{-0.2}$	$10.35^{+0.15}_{-0.20}$	1500^{+3800}_{-700}
152234	CH	-9.0 ± 0.4	$3.0^{+1.0}_{-1.0}$	$12.40^{+0.10}_{-0.10}$	7080^{+5510}_{-3930}
		-1.3 ± 0.2	$1.0^{+0.2}_{-0.2}$	$12.20^{+0.10}_{-0.20}$	790^{+350}_{-280}
		$+2.3 \pm 0.2$	$1.5^{+0.4}_{-0.3}$	$12.85^{+0.10}_{-0.10}$	1770^{+1070}_{-640}
	CH^+	-6.5 ± 0.5	$5.0^{+1.0}_{-1.0}$	$13.00^{+0.10}_{-0.15}$	19700^{+8700}_{-7100}
		-0.8 ± 0.2	$1.0^{+0.2}_{-0.3}$	$12.00^{+0.10}_{-0.10}$	790^{+350}_{-400}
		$+2.6 \pm 0.1$	$2.0^{+0.2}_{-0.2}$	$13.15^{+0.05}_{-0.10}$	3150^{+660}_{-600}
152235	CH	-5.7 ± 0.2	$1.4^{+0.2}_{-0.4}$	$13.28^{+0.07}_{-0.13}$	1540^{+1170}_{-760}
		-3.0 ± 0.3	$1.0^{+1.0}_{-0.3}$	$12.85^{+0.15}_{-0.20}$	790^{+2360}_{-400}
		$+0.5 \pm 0.3$	$2.0^{+0.3}_{-0.3}$	$13.05^{+0.10}_{-0.10}$	3150^{+1010}_{-870}
	CH^+	-5.1 ± 0.2	$1.8^{+0.2}_{-0.2}$	$13.58^{+0.05}_{-0.10}$	2550^{+600}_{-530}
		-2.3 ± 0.5	$1.5^{+2.0}_{-0.5}$	$12.55^{+0.40}_{-0.25}$	1770^{+7870}_{-980}
		$+0.6 \pm 0.3$	$3.0^{+0.5}_{-0.5}$	$13.15^{+0.10}_{-0.15}$	7080^{+2560}_{-2160}
152236	CH	-16.1 ± 0.5	$1.5^{+0.5}_{-0.5}$	$12.25^{+0.10}_{-0.20}$	1770^{+1380}_{-980}
		-10.0 ± 0.2	$1.0^{+0.8}_{-0.3}$	$12.45^{+0.20}_{-0.05}$	790^{+1760}_{-400}
		-9.0 ± 0.3	$3.0^{+1.0}_{-1.0}$	$12.75^{+0.10}_{-0.20}$	7080^{+5510}_{-3930}
		-1.5 ± 0.2	$1.5^{+1.0}_{-0.5}$	$12.40^{+0.10}_{-0.10}$	1770^{+3150}_{-980}
		$+0.9 \pm 0.1$	$0.8^{+0.1}_{-0.1}$	$13.05^{+0.03}_{-0.05}$	500^{+130}_{-120}
	CH^+	-15.3 ± 0.5	$3.6^{+0.9}_{-0.6}$	$12.40^{+0.15}_{-0.10}$	10200^{+5700}_{-3200}
		-8.0 ± 0.2	$2.2^{+0.2}_{-0.6}$	$12.87^{+0.06}_{-0.17}$	3810^{+720}_{-1290}
		-3.5 ± 0.3	$2.2^{+1.3}_{-0.7}$	$12.38^{+0.22}_{-0.23}$	3810^{+5830}_{-2040}
		$+2.0 \pm 0.2$	$2.0^{+0.7}_{-0.2}$	$12.65^{+0.15}_{-0.07}$	3150^{+2590}_{-600}
	CN R(0)	-10.4 ± 0.1	$0.6^{+0.2}_{-0.2}$	$11.40^{+0.10}_{-0.10}$	570^{+440}_{-310}
		$+0.5 \pm 0.1$	$0.6^{+0.1}_{-0.1}$	$12.20^{+0.05}_{-0.08}$	570^{+200}_{-170}
	CN R(1)	-10.2 ± 0.2	$0.6^{+0.2}_{-0.3}$	$11.20^{+0.10}_{-0.15}$	570^{+440}_{-420}
		$+0.4 \pm 0.1$	$0.6^{+0.1}_{-0.1}$	$11.78^{+0.07}_{-0.08}$	570^{+200}_{-170}
152270	CH	$+2.3 \pm 0.1$	$1.6^{+0.3}_{-0.3}$	$13.10^{+0.05}_{-0.08}$	2010^{+830}_{-680}
	CH^+	-14.8 ± 0.3	$2.5^{+0.5}_{-0.5}$	$12.55^{+0.10}_{-0.20}$	4920^{+2160}_{-1770}
		-4.2 ± 0.2	$0.9^{+0.3}_{-0.3}$	$12.20^{+0.20}_{-0.20}$	640^{+500}_{-350}
		$+2.4 \pm 0.2$	$2.3^{+0.2}_{-0.3}$	$13.15^{+0.05}_{-0.10}$	4160^{+760}_{-1010}
	CN R(0)	$+2.1 \pm 0.1$	$0.7^{+0.1}_{-0.2}$	$11.95^{+0.05}_{-0.15}$	770^{+240}_{-380}
	CN R(1)	$+2.0 \pm 0.2$	$0.6^{+0.2}_{-0.2}$	$11.60^{+0.15}_{-0.20}$	570^{+440}_{-310}

3.2 Line profiles

The primary aim of the present work was to determine the intrinsic profiles of the interstellar molecular lines, and to this end a line profile analysis was performed using the DIPSO spectrum analysis program (Howarth & Murray 1988). The theoretical line profiles include the Λ-doubling in the CH line (separation 1.43 km s^{-1}), and the unresolved rotational substructure within the CN R(0) and R(1) lines (see Crawford et al. 1994 for further details), and the hyperfine splitting in the K I line (separation 0.35 km s^{-1}). The model profiles were convolved with the instrumental response function (although the UHRF resolution is sufficiently high that this was found to have a very small effect), and compared interactively with the observed data. The best-fitting theoretical line profiles are superimposed on the observed spectra in Figs 1–5, and the resulting line-profile parameters (heliocentric velocity, velocity dispersion and column density) are given in Table 3. The errors tabulated in Table 3 give the range of these parameters which were found to give acceptable fits to the observed profiles. Table 3 also gives the values of the kinetic temperature corresponding to the observed linewidths; these values have been derived by assuming that there is no turbulent contribution to the line profiles, and so they are strict upper limits to the actual kinetic temperatures of the atoms and molecules in these interstellar clouds.

3.2.1 Velocity structure

The CH and CH^+ spectra of the four Sco OB1 stars are qualitatively similar in terms of their velocity structure, with each CH component generally being associated with a CH^+ component of comparable strength (Figs 2–5). For the two stars that have been observed in CN (Table 3; Figs 4 and 5), this molecule occurs at essentially the same velocity as the strongest CH component(s). Minor differences between the CH and CH^+ line profiles are found for HD 152236, which has a weak CH component at -10 km s^{-1} with no corresponding CH^+, and HD 152270, which exhibits weak CH^+ components at -14.8 and -4.2 km s^{-1} which are not present in CH. The reality of the latter two features may be questioned, as they are not clearly present in any of the individual frames which were co-added to produce the final spectrum. However, the fact that weak features at these velocities can be discerned in the lower resolution spectra of Crawford (1989a; his fig. 7) may lend them some credibility. If accepted at face value, the -4.2 km s^{-1} CH^+ component is of special interest, as it is the only well-resolved CH^+ component with a *b*-value $\lesssim 1$ km s^{-1} (Table 3), which would imply a temperature at the very low end of the range necessary for CH^+ production through reaction (1).

The Coalsack star, HD 110432, has a rather different velocity structure, with two CH components, but only one CH^+ component at an intermediate velocity. This star was also observed in Ca K and K I (Table 3; Figs 1c and d), and there is generally good agreement between the atomic and molecular velocity structure. The most interesting points to note are (i) that the weaker ($+2.9$ km s^{-1}) CH component breaks up into two K I components, (ii) that the main Ca K component occurs at the velocity of the CH^+ line, and (iii) that the strongest K I component occurs at the velocity of the strongest CH component. A detailed discussion of the

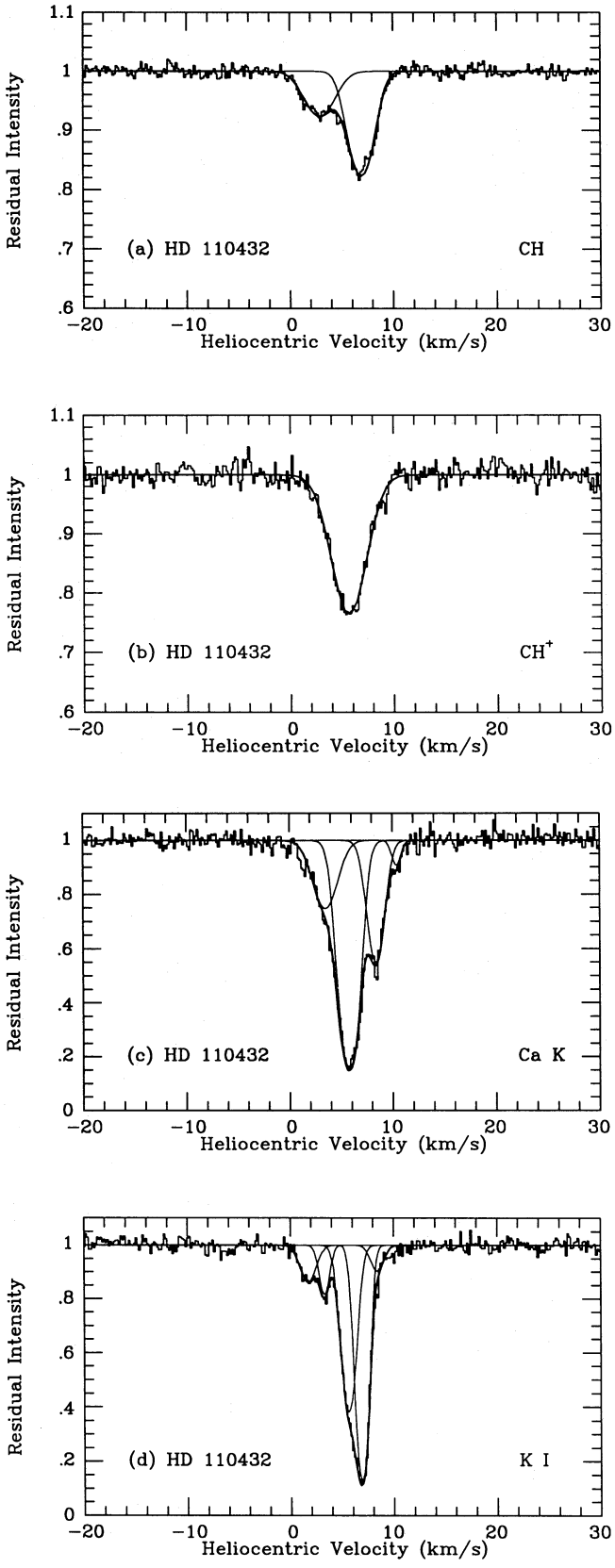

Figure 1. The interstellar lines observed towards HD 110432. The observed data are plotted as histograms. The smooth curves are theoretical line profiles with the parameters given in Table 3. Where multiple velocity components are blended, the individual line profiles are also shown.

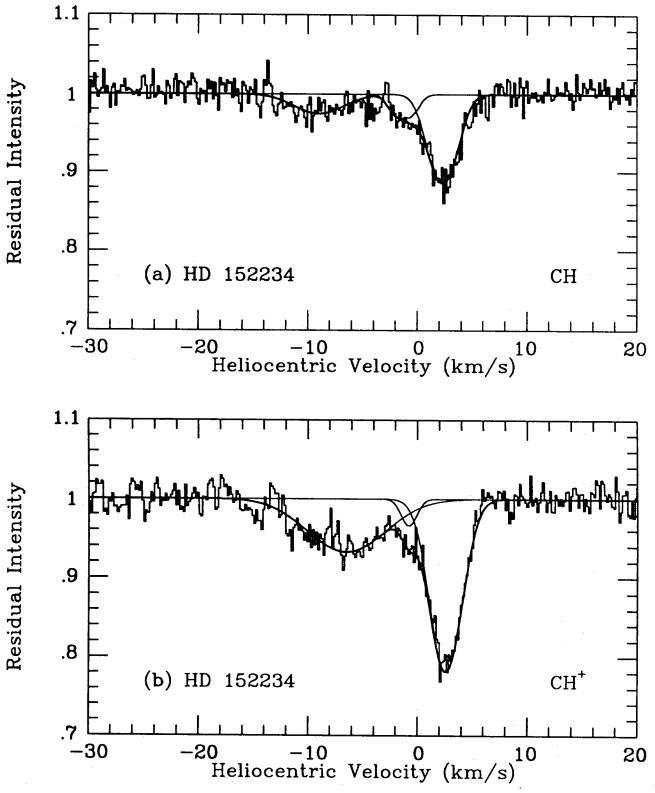

Figure 2. The interstellar lines observed towards HD 152234. For details see caption to Fig. 1.

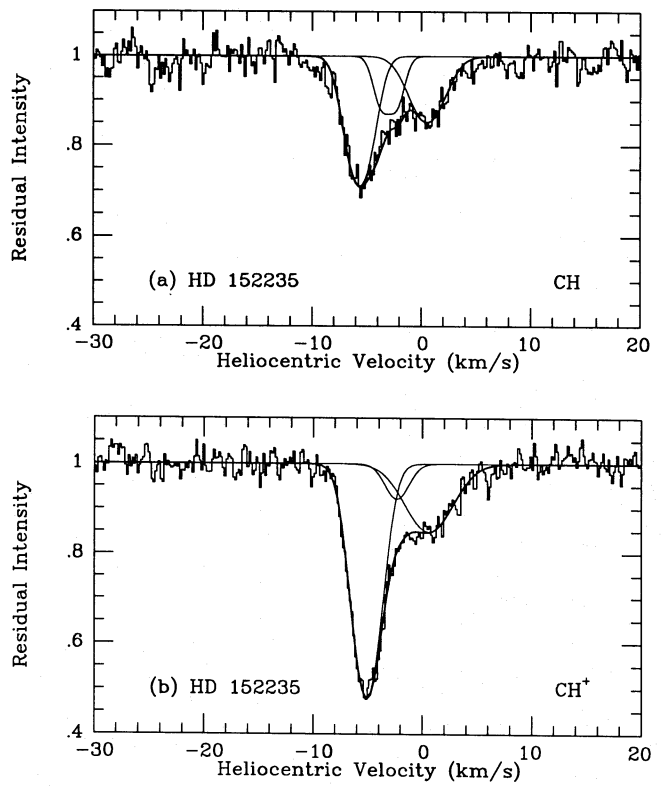

Figure 3. The interstellar lines observed towards HD 152235. For details see caption to Fig. 1.

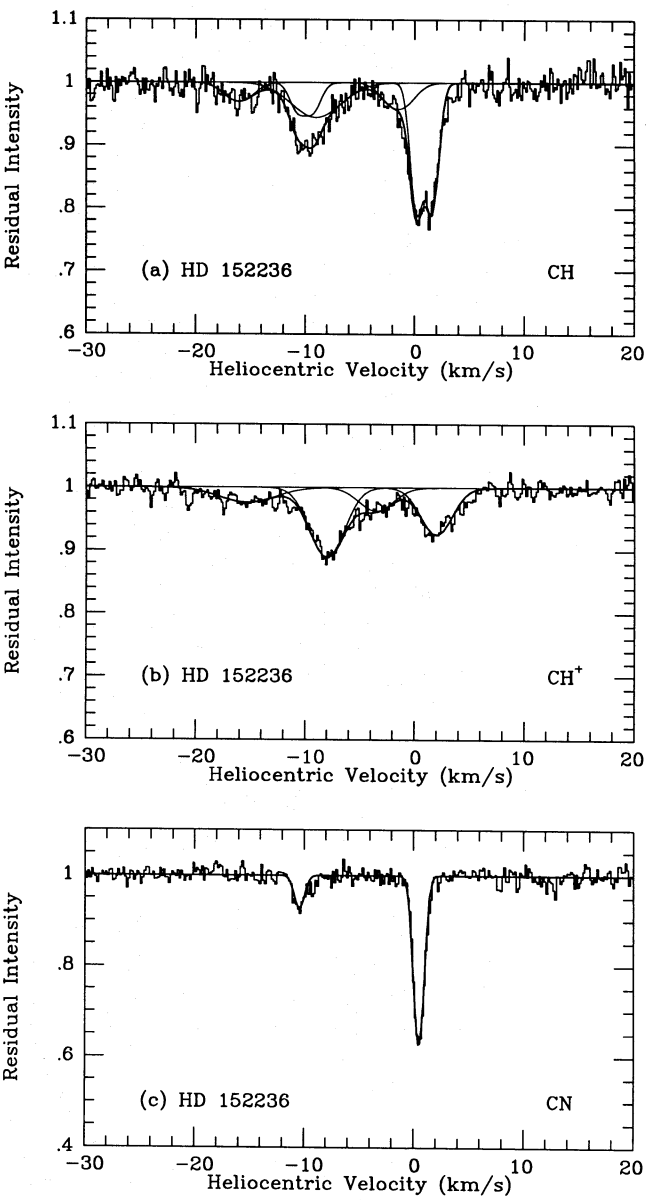

Figure 4. The interstellar lines observed towards HD 152236. For details see caption to Fig. 1.

implications of the velocity structure towards this star is deferred until Section 4.2.

Table 4 groups together those components towards the Sco OB1 stars which were identified in both CH and CH^+, and lists the velocity differences between the two species. It will be seen that in all cases the velocity difference between CH and CH^+ is very small. In particular, of the strongest, and therefore best defined, molecular components (underlined in Table 4), only that towards HD 152236 has a velocity difference as large as 1 km s^{-1}. There is no significant velocity shift at all in the case of HD 152270, and barely any for the main components towards HD 152234 and 152235. If we consider the weaker components listed in Table 4, we see that in only two cases is the velocity difference $\gtrsim 2$ km s^{-1}, and the significance of both of these may be doubted: the -9.0 km s^{-1} CH component

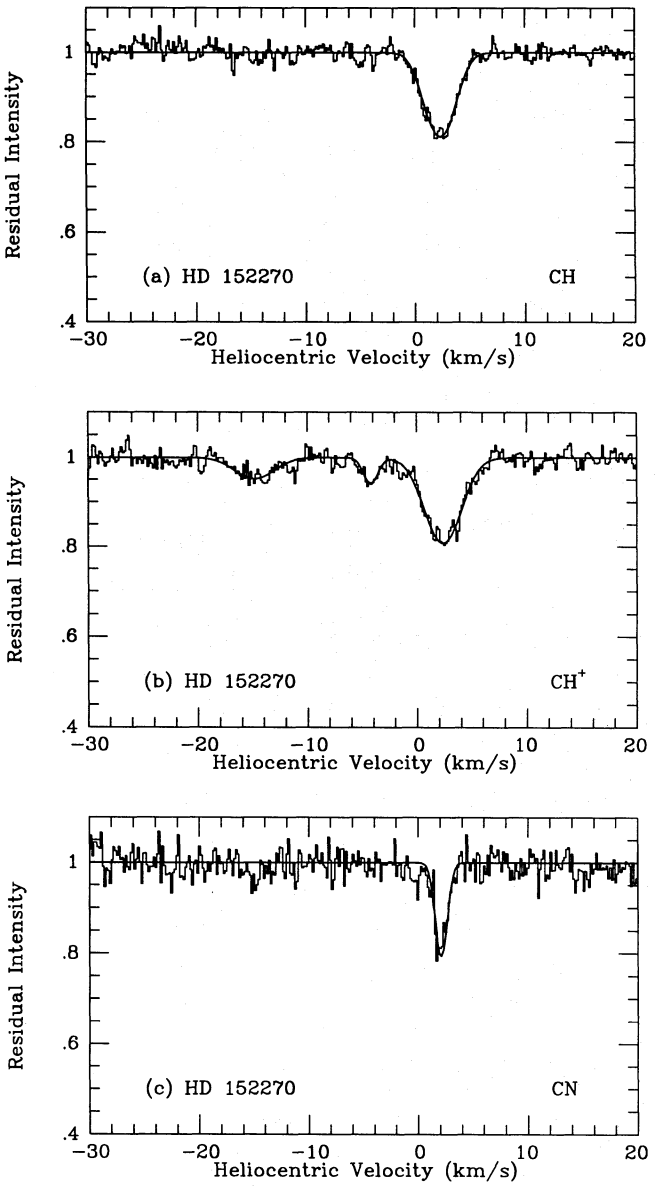

Figure 5. The interstellar lines observed towards HD 152270. For details see caption to Fig. 1.

towards HD 152234 is very shallow and much broader than the others, while the -1.5 km s^{-1} CH and -3.5 km s^{-1} CH$^+$ components towards HD 152236 are both blended with much stronger components on either side.

These velocity differences agree well with those found in the earlier study of Crawford (1989a; cf. his table 5 and 'note added in proof'). In particular, the sign of the velocity shift is the same, with CH$^+$ having a slightly more positive velocity. As noted by Crawford (1989a), this may be due to a small error in the adopted rest wavelengths. For example, Carrington & Ramsey (1982) state an uncertainty of 0.02 cm^{-1} on their determination of the wavenumbers used to derive the rest wavelength of the CH$^+$ line adopted by Lambert & Danks (1986) and employed here (Table 1), which corresponds to a velocity uncertainty of 0.25 km s^{-1}.

3.2.2 *Velocity dispersions*

All of these lines of sight have been studied previously using the Mt Stromlo coudé echelle spectrograph at a resolving power of $R = 10^5$ (Section 1.1), and it is of interest to compare the measurements of the velocity dispersions. As discussed in Section 1, a resolving power of 10^5 is insufficient fully to resolve the intrinsic linewidths, and in the earlier work the b-values were obtained by modelling the effect of the relatively broad instrumental profile. Comparison of the present results (Table 3) with the earlier ones (tables 3 and 4 of Crawford 1989a, table 2 of Crawford 1990, and table 1 of Crawford 1991a) shows that the UHRF-derived b-values generally fall within the (rather broad) errors quoted on the Mt Stromlo data, but that, as one would expect, the present values are much more tightly constrained. In terms of the results of other authors, we note that the range of CH$^+$ b-values obtained here (roughly 1.5–3.5 km s^{-1} for well-defined components) is similar to that deduced by Lambert & Danks (1986) for a large sample of southern stars (although the accuracy of their b-values was limited by the need to deconvolve the comparably broad instrumental profile).

It is particularly noteworthy that the present b-values have well-defined *lower* limits. At $R = 10^5$ the instrumental b-value is 1.8 km s^{-1}, and this made it difficult in the earlier work to determine whether any of the components had b-values $\lesssim 1.2$ km s^{-1}. On the basis of the UHRF data, we now see that, with the exception of the strongest CH component towards HD 152236 ($b = 0.8 \pm 0.1$ km s^{-1}), none of the CH and CH$^+$ components is significantly narrower than this. On the other hand, the new data have conclusively shown that the CN lines are very much narrower. Whereas the Mt Stromlo data were only able to assign an upper limit of 1.2 km s^{-1} for the CN b-values towards HD 152236 and 152270 (Crawford 1990), the new data show that the CN lines are actually only half as broad as the earlier upper limit (Table 3). It is of interest to note that the CN b-values measured here (≈ 0.6 km s^{-1}) are consistent with the range (0.4–1.0 km s^{-1}) obtained by Gredel, van Dishoeck & Black (1991) for 16 southern stars by comparing the equivalent widths of the R(0) lines in the red and violet systems of this molecule.

Table 4 gives the ratio of the CH$^+$ and CH velocity dispersions, and it will be seen that, with the exception of one poorly defined (because badly blended) component towards HD 152236, this ratio is generally greater than unity. It is true, given the errors, that this result appears to be only marginally significant in most individual cases, but it is highly significant in the mean (excluding the uncertain component towards HD 152236, the weighted mean value of this ratio is 1.41 ± 0.13). As CH and CH$^+$ have identical masses, this result definitely shows that the CH$^+$ resides in hotter and/or more turbulent regions of the clouds. Although long suspected, this result had only been previously demonstrated in the case of ζ Oph (Lambert et al. 1990; Crawford et al. 1994), all other studies having lacked the spectral resolution needed to prove it unambiguously.

It is also of interest to determine whether the velocity dispersions of CH and CN are consistent with these molecules existing in the same regions of the absorbing clouds. As the CN molecule is twice as heavy as CH, we

Table 4. Velocity shifts, and b-value and column density ratios for corresponding CH and CH^+ velocity components towards the Sco OB1 stars. The strongest, and therefore best-defined, components towards each star are underlined for clarity. In order to calculate the ratios and their errors, mean b- and N-values were obtained from the (generally asymmetric) error limits listed in Table 3, and the numerator and denominator errors were propagated in quadrature.

Star (HD)	v(CH) (km s^{-1})	$v(CH^+)$ (km s^{-1})	$[v(CH) - v(CH^+)]$ (km s^{-1})	$b(CH^+)/b(CH)$	$N(CH^+)/N(CH)$
152234	-9.0 ± 0.4	-6.5 ± 0.5	-2.5 ± 0.6	1.7 ± 0.7	3.8 ± 1.4
	-1.3 ± 0.2	-0.8 ± 0.2	-0.5 ± 0.3	1.0 ± 0.3	0.7 ± 0.3
	$+2.3 \pm 0.2$	$+2.6 \pm 0.1$	-0.3 ± 0.2	1.3 ± 0.3	1.9 ± 0.5
152235	-5.7 ± 0.2	-5.1 ± 0.2	-0.6 ± 0.3	1.4 ± 0.4	2.0 ± 0.6
	-3.0 ± 0.3	-2.3 ± 0.5	-0.7 ± 0.6	1.7 ± 1.2	0.8 ± 0.6
	$+0.5 \pm 0.3$	$+0.6 \pm 0.3$	-0.1 ± 0.4	1.5 ± 0.3	1.2 ± 0.4
152236	-16.1 ± 0.5	-15.3 ± 0.5	-0.8 ± 0.7	2.5 ± 1.0	1.6 ± 0.7
	-9.0 ± 0.3	-8.0 ± 0.2	-1.0 ± 0.4	0.7 ± 0.3	1.3 ± 0.5
	-1.5 ± 0.2	-3.5 ± 0.3	$+2.0 \pm 0.4$	1.4 ± 0.8	1.0 ± 0.6
	$+0.9 \pm 0.1$	$+2.0 \pm 0.2$	-1.1 ± 0.2	2.8 ± 0.7	0.5 ± 0.1
152270	$+2.3 \pm 0.1$	$+2.4 \pm 0.2$	-0.1 ± 0.2	1.4 ± 0.3	1.1 ± 0.2

Table 5. The CN/CH velocity dispersion ratio, and CN excitation temperature, T_{10}, for components detected in CN. For error estimates, see caption to Table 4.

Star (HD)	v_{helio}(CN) (km s^{-1})	b(CN)/b(CH)	T_{10} (K)
152236	-10.4	0.48 ± 0.26	3.4 ± 0.8
152236	$+0.5$	0.75 ± 0.16	2.7 ± 0.3
152270	$+2.1$	0.41 ± 0.12	3.0 ± 0.8

expect $b(CN)/b(CH) = 1/\sqrt{2}$ in the absence of turbulence. As turbulence begins to dominate, this ratio tends to unity, so for molecules located in the same region of the cloud we expect $0.71 \leq b(CN)/b(CH) \leq 1.0$. The $b(CN)/b(CH)$ ratios for the three components observed in CN in the present work are given in Table 5. It will be seen that this ratio is consistent with the two molecules co-existing spatially in the cloud responsible for the main ($+0.5$ km s^{-1}) component towards HD 152236, but is barely so for the weaker (-10.4 km s^{-1}) component towards this star, and is inconsistent with this view in the case of HD 152270. Thus the present observations have definitely proved that the CN exists in a colder and/or less turbulent region than the bulk of the CH in the cloud responsible for the main component towards HD 152270. As it has long been thought that CN occurs predominantly in the cold cores of diffuse molecular clouds (e.g. Federman, Danks & Lambert 1984), or in the shielded inner regions of dense cloud envelopes (Federman et al. 1994), this result is not unexpected, but, again, it has taken the UHRF resolution to demonstrate it from an analysis of the line profiles.

3.3 The CN excitation temperature

The observation of both the R(0) and R(1) lines of CN makes it possible to calculate the excitation temperature of this molecule from the observed column densities of the $N=0$ and $N=1$ rotational levels. The excitation temperatures are given in Table 5, and all of these are consistent with the *COBE*-derived value of 2.74 ± 0.06 K for the microwave background (Mather et al. 1990). However, we note that the value obtained for the -10.4 km s^{-1} component towards HD 152236 is only marginally consistent with excitation by the microwave background, and may represent a case where collisional excitation has raised the excitation temperature to a higher value. Black & van Dishoeck (1991) have shown that this effect is likely to become important for densities greater than few thousand molecules cm^{-3}, so this component may arise in a denser cloud than those giving rise to the other CN components. Clearly, if this interpretation is correct, the path-length through this cloud must be short, in order to reconcile a high spatial density with a low column density.

4 DISCUSSION: IMPLICATIONS FOR THE CH^+ PROBLEM

4.1 The Sco OB1 stars

The first thing to note is that the line profiles of the Sco OB1 stars are in qualitative disagreement with the shock model predictions: both the hydrodynamic and MHD models predict a single broad CH^+ component, as this molecule is formed only in the hot post-shock gas, but they predict a minimum of two CH components, arising in the hot post-shock and the cold post-shock gas, respectively. In contrast, apart from the minor discrepancies found for HD 152236 and 152270 (discussed in Section 3.2.1), we find that every CH^+ component towards the Sco OB1 stars is associated with one CH component (Table 4), which is not readily explicable in terms of the shock models.

In addition to these qualitative discrepancies, there are also significant quantitative discrepancies between the observations and the shock model predictions outlined in Section 1.2. First, as noted by Crawford (1989a), and confirmed by the present observations, the very small velocity differences between the strongest CH and CH^+ components ($\lesssim 1$ km s^{-1}; Table 4) are inconsistent with the predictions of non-MHD shock models unless there is a large angle ($\theta \gtrsim 70°$) between the line of sight and the direction of shock propagation. In the case of the MHD models, it is true that a velocity shift of the order of only 1 km s^{-1} (and less for large θ) is expected between the CH^+ and the cold post-shock gas, and that this might be consistent with the observed shifts in several cases (Table 4). However, as the models of Draine & Katz (1986) also predict a hot post-shock component in CH, for which $N(CH)/N(CH^+) \approx 5$ in a non-enhanced interstellar radiation field,[1] identification of the comparably strong CH^+ and CH components with the shock and cold post-shock gas, respectively, would lead us to expect an additional, and much stronger, CH component offset by several km s^{-1}. This is not observed: in all cases except HD 152236, the strongest CH^+ component corresponds (to within less than 1 km s^{-1}) with the *strongest* CH component. Not only are the observed column density ratios incompatible with the MHD model predictions (Table 4), but the velocity agreement is explicable only by postulating a very large angle between the line of sight and the shock direction for all of the observed stars. In the case of HD 152270, and the main component towards HD 152234, for which the velocity difference between the two species is negligible, the angle θ would have to be about 90°, which is inconsistent with the line of sight passing through regions dominated by both CH and CH^+. In the case of HD 152236, the main CH component (which is associated with its own weak CH^+ absorption) is offset by 9 km s^{-1} from the strongest CH^+ component (Fig. 4), which is too great a velocity difference to be explained in terms of a shock model.

On the other hand, it *is* true that the ratio of the *b*-values (Table 4) indicates that the CH^+ is produced in hotter and/or more turbulent gas than the CH, and that the temperatures deduced from the CH^+ line profiles (Table 3) are consistent with those needed to drive reaction (1). As discussed in Section 1.2, shocks are not the only means by which the temperature of a molecular gas may be raised to several thousand degrees. In particular, as the hot interior of the Sco–Cen bubble almost certainly comes into contact with the Lupus molecular clouds, the outskirts of which are the most probable location for the main molecular components observed towards the Sco OB1 stars (Section 1.1), the suggestion that CH^+ forms in warm boundary layers between cold molecular gas and a hot intercloud medium (Duley et al. 1992) is particularly attractive in the present context. Quantitative models of the chemistry in such interface regions have not yet been produced, but Duley et al. (1992) have shown that there is quite a wide range of temperature, density, and radiation field strength that would be capable of producing the observed CH^+ column densities for sufficiently thick boundary layers.

The calculations of Duley et al. also predict the $n(CH)/n(CH^+)$ abundance ratio, and in principle this could be used to decide which of the models is closest to the observations. However, there is a complication in that the ratio given by the models refers only to the hot gas in the boundary layer itself, whereas the line of sight will also sample cold CH in the background cloud. As the boundary layer is probably no thicker than about 10 per cent of the cloud radius (Duley et al. 1992), and as the presence of CN indicates a significant molecular concentration in the background cloud, we might expect $N(CH)$ to be significantly greater than $N(CH^+)$, whereas the observed $N(CH)/N(CH^+)$ ratio is about unity for most of these components (Table 4). There are two possible explanations for this, which are not mutually exclusive. First, we would expect that in the cloud interior some of the CH will have been processed into other molecules, including CN (e.g. Federman et al. 1994), thereby reducing its abundance in the interior. In addition, it may be that the $N(CH)/N(CH^+)$ ratio in the boundary layer itself is much less than unity, corresponding to the low-pressure models of Duley et al. For example, for $\chi = 1$, $T = 2000$ K and $nT = 4000$ cm^{-3} K, the models give $n(CH)/n(CH^+) = 2.2 \times 10^{-2}$ for the boundary layer, which would permit the CH column density of the background cloud to be 45 times greater than that of the boundary layer, while maintaining an overall $N(CH)/N(CH^+)$ ratio of about one, as observed.

4.2 HD 110432

Of the five stars studied here, HD 110432 is the most unusual in having two unequally strong CH velocity components, but only one (perfectly symmetrical) CH^+ component at an intermediate velocity. Moreover, although the CH^+ component is broader than either of the two CH components, it is narrower than the two combined, and cannot be modelled as two unresolved subcomponents with the velocities of the CH components. This star was also observed in Ca II and K I and, as discussed in Section 3.2.1, it is noteworthy that the strongest Ca II component coincides with the CH^+ component, whereas the strongest K I component coincides with the strongest CH component, although there is a weaker K I component at the CH^+ velocity (Table 3). This velocity structure is illustrated in Fig.

[1]This large ratio is a consequence of the high fractional abundance of H_2 adopted in the models of Draine & Katz, which might be unrealistic. However, as there is quite convincing evidence that the strongest components observed here are formed in the vicinity of dense (CO-emitting) molecular clouds, it seems that a high H_2/H ratio in the pre-shock gas may well be appropriate for these clouds.

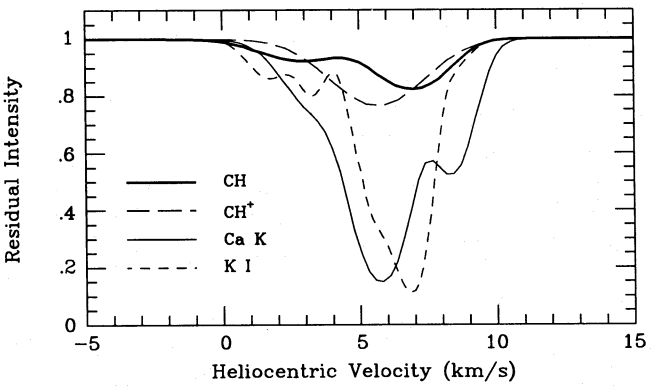

Figure 6. The best-fitting line-profile models for the atomic and molecular lines observed towards HD 110432 (Table 3), plotted on an expanded scale to show the complex velocity structure in the line of sight through the Coalsack (see text for discussion).

6, which shows the best-fitting model line profiles overplotted on an expanded scale.

Of the five interstellar sightlines studied in this work, this is the one in which the CH and CH^+ line profiles appear, at first sight, closest to the predictions of the shock models. As we saw in Section 1.2, in the case of an MHD shock we expect the hot CH^+ to occur at an intermediate velocity between CH components formed in the hot post-shock and cold post-shock gas [cf. section III(b) of Draine & Katz 1986]. Moreover, for a 10 km s^{-1} shock moving away from the observer, the predicted velocity shifts are remarkably similar to those actually observed for HD 110432. In this case, the models of Draine & Katz (their fig. 4) suggest that, relative to the pre-shock gas, the hot CH will be redshifted by 3.8 km s^{-1}, the CH^+ by 7.3 km s^{-1}, and the cold post-shock gas by 8.5 km s^{-1}. Thus the predicted velocity differences between the least redshifted CH component and the CH^+ (3.5 km s^{-1}), and between the CH^+ and the more redshifted CH component (1.2 km s^{-1}), are very close (actually identical in one case) to the observed shifts of 2.8 and 1.2 km s^{-1}, respectively.

However, while at first sight the CH and CH^+ line profiles appear to be in good agreement with the detailed predictions of the model of Draine & Katz, there are actually a number of reasons why it is very unlikely that the velocity structure observed towards HD 110432 is due to a shock. These reasons are itemized below.

(i) The MHD models predict that the hot post-shock CH (which on this interpretation would correspond to the +2.9 km s^{-1} component towards HD 110432) will have a significantly broader line profile than the CH^+, and reference to Fig. 1 and Table 3 shows that this is not the case. Not only does the model fail qualitatively, it specifically predicts *b*-values of 2.7 km s^{-1} for the hot CH and 1.8 km s^{-1} for the CH^+; while the observed value for CH^+ (2.3 ± 0.2 km s^{-1}) is not too different from this prediction, the observed CH *b*-value (1.7 ± 0.2 km s^{-1}) is very significantly narrower.

(ii) The models of Draine & Katz predict that, in addition to being broad, the hot post-shock CH will produce a distinctly flat-bottomed, strongly non-Gaussian, line profile. From their fig. 5 we see that the flat core of the line profile is expected to extend over a velocity range of about 4 km s^{-1}, and there is no doubt that the UHRF would have resolved this distinctive line profile had it been present.

(iii) The Draine & Katz models also make predictions concerning the CH/CH^+ column density ratio for the hot post-shock gas. This ratio is quite sensitive to the adopted value of χ, the enhancement factor of the interstellar ultraviolet radiation field. For their preferred models, Draine & Katz adopt $\chi = 3$, which predicts approximately equal column densities of CH and CH^+. However, as the interstellar lines towards HD 110432 arise in the Coalsack (Crawford 1989b, 1991a), and given that the star itself lies well in the background, there is no reason to assume $\chi > 1$ in this case (and $\chi < 1$ may be more appropriate, given the likelihood of shielding by the dark Coalsack material). For the case where $\chi = 1$, the models predict $N(CH)/N(CH^+) \approx 5$ for the hot post-shock gas, which is in disagreement with the observed ratio of $0.28^{+0.07}_{-0.06}$.

(iv) Finally, we note that the +2.9 km s^{-1} CH component, which on the shock model interpretation would arise in the hot post-shock region, is resolved into two discrete velocity components in the K I spectrum (see Fig. 6). The shock models provide no natural explanation for this, which would be better explained on the view that the two K I components arise in relatively dense clumps within the Coalsack which share a common CH envelope (see below).

Taken together, these arguments suggest that the CH and CH^+ line profiles towards HD 110432 do not result from the action of an MHD shock. On the other hand, as discussed by Crawford (1991a), the velocity structure observed in CH can plausibly be explained in terms of the internal structure of the Coalsack determined by the CO mm-wave observations by Nyman, Bronfman & Thaddeus (1989; cf. their fig. 4), with the two CH components being formed when the line of sight passes relatively close ($\lesssim 0.5$ pc) to dense, CO-emitting, gas within the Coalsack. At a velocity intermediate between the two CH components, the line of sight appears to miss the dense gas by more than a parsec, and therefore presumably samples an outer region of the cloud envelope. This is consistent with the suggestion that CH^+ is produced in a warm boundary layer between the cold molecular gas of the Coalsack and the hot interior of the Sco–Cen bubble (cf. Section 1.1).

This interpretation is supported by the observation that the strongest Ca II component occurs at the same velocity (to within 0.1 km s^{-1}; cf. Table 3) as the CH^+ component. Barlow et al. (1995) have argued that Ca^+ occurs preferentially in warm haloes surrounding cooler gas, owing to the enhanced desorption of Ca atoms from grain surfaces at temperatures of several thousand degrees. This is exactly the kind of environment where CH^+ is expected to form according to the interface model of Duley et al. (1992), and we see from Table 3 that the *b*-values are consistent with both species co-existing in a gas with a temperature in the range 3500–5000 K. As CH is expected to occur at a different location (deeper into the cloud), we have no reason to expect that the CH components will have exactly the same velocities as the other (weaker) Ca^+ components, but inspection of Fig. 6 does seem to imply that the Ca depletion is greater (i.e., the absorption is weaker) where the CH absorption (and therefore the density) is higher. The same trend was observed by Cardelli, Federman & Smith (1991), and is consistent with the view that Ca is depleted from the gas phase in dense (molecular) regions owing to adsorption on to grain surfaces.

On the other hand, owing to its small adsorption binding

energy, K I (like Na I) is not expected to undergo significant gas-phase depletion or subsequent desorption from grains (Barlow 1978), and may be expected to trace both the warm and cool gas (with the caveat that it will start to be destroyed by collisional ionization at temperatures above a few thousand degrees K). This is fully consistent with the fact that we can identify a K I component with each of the components observed in CH and CH^+, and with all but the weakest Ca II component (Table 3; Fig. 6). However, it is true that the *b*-value of the $+5.6$ km s^{-1} K I component is not consistent with a temperature quite as high as that deduced from the CH^+ line profile, possibly owing to the collisional ionization of K I in the warmest regions contributing the CH^+. Finally, the fact that the $+2.9$ km s^{-1} CH component breaks up into two K I components may be explained by supposing that the line of sight has here passed through two relatively dense clumps, which either are both surrounded by CH haloes (giving blended components in the present spectrum), or share a common CH envelope.

5 CONCLUSIONS

The UHRF has been used to obtain ultra-high-resolution (0.3 km s^{-1} FWHM) observations of interstellar molecular lines towards five southern stars. Observations of interstellar Ca K and K I were also obtained in one case. These observations have fully resolved the intrinsic interstellar line profiles towards these stars for the first time, and the main conclusions are as follows.

(i) The resolution of the intrinsic line profiles has enabled us to make accurate measurements of velocity dispersions (*b*-values) of the various atomic and molecular components (Table 3). This has enabled us to show that for most components the CH^+ must exist in a hotter and/or more turbulent medium than the CH. The temperatures deduced from the CH^+ line profiles ($\gtrsim 2000$ K; Table 3) are consistent with CH^+ being formed through the endothermic ion–molecule reaction between C^+ and H_2 (reaction 1).

(ii) On the other hand, the CN components are much narrower than the corresponding CH components ($b \approx 0.6$ km s^{-1}; Table 3). In the case of the main component towards HD 152270, this is sufficient to prove that the CN must exist in a colder and/or less turbulent medium than CH (cf. Table 5). Thus, for this particular sightline, the present observations conclusively demonstrate that the cloud responsible for the strongest absorption components has an onion-shell structure: the CN occurs in the coolest and/or least turbulent region (presumably the deep interior, as expected for a molecule strongly susceptible to photodissociation), CH occurs in a somewhat warmer and/or more turbulent region, while CH^+ occurs in the warmest and/or most turbulent regions of all.

(iii) For the four stars which are members of the Sco OB1 association (HD 152234, 152235, 152236 and 152270), we confirm earlier work at lower resolution, which showed that essentially every CH component has a corresponding (and comparably strong) CH^+ component, and that there is a very small ($\lesssim 1$ km s^{-1}) velocity difference between them (Table 4). Both the qualitative similarity of the CH and CH^+ line profiles and the magnitude of the velocity shifts between corresponding components conflict with the predictions of shock models for the production of CH^+ unless a large angle ($\gtrsim 70°$) is postulated between the line of sight and the direction of shock propagation. In the case of the main components present towards HD 152234 and 152270, this angle would have to be almost 90°, which would be inconsistent with the line of sight sampling both species behind the shock front. In the case of the star behind the Coalsack (HD 110432), the velocity structure (with CH^+ occurring at an intermediate velocity between two CH components) is superficially consistent with that predicted by MHD shock models, but strong arguments against a shock model interpretation also exist for this sightline (Section 4.2).

(iv) Given that shock models seem to be excluded by the present data, but that CH^+ is shown to occur in a hotter and/or more turbulent medium than the other molecules, it is suggested that this molecule is probably produced in a warm boundary layer between a hot intercloud medium and cold molecular gas (as proposed by Duley et al. 1992). This explanation is especially attractive in the present context, as there is considerable evidence (Section 1.1) that the hot interior of the Sco–Cen bubble must come into contact with both the Lupus molecular clouds (the outskirts of which are probably responsible for the main interstellar components towards the Sco OB1 association) and the Southern Coalsack (which is responsible for the lines observed towards HD 110432).

(v) As detailed chemical models of the interface regions between the coronal phase of the interstellar medium (such as the interior of the Sco–Cen bubble) and the cool molecular clouds embedded within it have not yet been produced, this may be a fruitful new direction for theoretical models of interstellar clouds.

ACKNOWLEDGMENTS

I thank S. K. Dunkin for reducing the 1993 CH spectrum of HD 152236. I am grateful to M. J. Barlow, and the referee, for critical readings of the original manuscript.

REFERENCES

Barlow M. J., 1978, MNRAS, 183, 417
Barlow M. J., Crawford I. A., Diego F., Dryburgh M., Fish A. C., Howarth I. D., Spyromilio J., Walker D. D., 1995, MNRAS, 272, 333
Black J. H., 1988, Adv. Atom. Mol. Phys., 25, 477
Black J. H., van Dishoeck E. F., 1988, ApJ, 331, 986
Black J. H., van Dishoeck E. F., 1991, ApJ, 369, L9
Cardelli J. A., Federman S. R., Smith V. V., 1991, ApJ, 381, L17
Carrington A., Ramsey D. A., 1982, Phys. Scripta, 25, 272
Cox D. P., Reynolds J., 1987, ARA&A, 25, 303
Crawford I. A., 1989a, MNRAS, 241, 575
Crawford I. A., 1989b, Observatory, 109, 232
Crawford I. A., 1990, MNRAS, 244, 646
Crawford I. A., 1991a, A&A, 246, 210
Crawford I. A., 1991b, A&A, 247, 183
Crawford I. A., 1992, MNRAS, 254, 264
Crawford I. A., Barlow M. J., Blades J. C., 1989, ApJ, 336, 212
Crawford I. A., Barlow M. J., Diego F., Spyromilio J., 1994, MNRAS, 266, 903
Dalgarno A., 1976, in Burke P. G., Moiseiwitsch B. L., eds, Atomic Processes and Applications. North-Holland, Amsterdam, p. 110

Dame T. M. et al., 1987, ApJ, 322, 706
de Geus E. J., 1992, A&A, 262, 258
de Geus E. J., de Zeeuw P. T., Lub J., 1989, A&A, 216, 44
Diego F., 1993, Applied Optics, 32, 6284
Diego F. et al., 1995, MNRAS, 272, 323
Draine B. T., Katz N. S., 1986, ApJ, 310, 392
Duley W. W., Hartquist T. W., Sternberg A., Wagenblast R., Williams D. A., 1992, MNRAS, 255, 463
Egger R. J., Aschenbach B., 1995, A&A, 294, L25
Elitzur M., Watson W. D., 1978, ApJ, 222, L141
Elitzur M., Watson W. D., 1980, ApJ, 236, 172
Falgarone E., Puget J.-L., 1995, A&A, 293, 840
Falgarone E., Pineau des Forêts G., Roueff E., 1995, A&A, in press
Federman S. R., Danks A. C., Lambert D. L., 1984, ApJ, 287, 219
Federman S. R., Strom C. J., Lambert D. L., Cardelli J. A., Smith V. V., Joseph C. L., 1994, ApJ, 424, 772
Fich M., Blitz L., Stark A. A., 1989, ApJ, 342, 272
Franco G. A. P., 1989, A&A, 215, 119
Gredel R., van Dishoeck E. F., Black J. H., 1991, A&A, 251, 625
Gredel R., van Dishoeck E. F., Black J. H., 1993, A&A, 269, 477
Howarth I. D., Murray J., 1988, Starlink User Note, No. 50
Humphreys R. M., 1978, ApJS, 38, 309
Lambert D. L., Danks A. C., 1986, ApJ, 303, 401
Lambert D. L., Sheffer Y., Crane P., 1990, ApJ, 359, L19
Mather J. C. et al., 1990, ApJ, 354, L37
Mitchell G. F., Watt G. D., 1985, A&A, 151, 121
Morton D. C., 1991, ApJS, 77, 119
Murphy D. C., Cohen R., May J., 1986, A&A, 167, 234
Nyman L. Å., Bronfman L., Thaddeus P., 1989, A&A, 216, 185
Palazzi E., Mandolesi N., Crane P., 1992, ApJ, 398, 53
Pineau des Forêts G., Flower D. R., Hartquist T. W., Dalgarno A., 1986, MNRAS, 220, 801
Rodgers A. W., 1960, MNRAS, 120, 163
Shortridge K., 1988, Starlink Users Note, No. 86
Spitzer L., 1978, Physical Processes in the Interstellar Medium. John Wiley, New York